PAPER • **OPEN ACCESS**

Numerical analysis of the bulge test in temperature for the EN AW 6061-T6 sheet

To cite this article: A Boyer *et al* 2020 *IOP Conf. Ser.: Mater. Sci. Eng.* **967** 012024

IOP Conf. Series: Materials Science and Engineering **967** (2020) 012024 doi:10.1088/1757-899X/967/1/012024

Numerical analysis of the bulge test in temperature for the EN AW 6061-T6 sheet

A Boyer[1,2,*], L Germain[1], H Laurent[1], D M Neto[2] and M C Oliveira[2]

[1]Univ. Bretagne Sud, UMR CNRS 6027, IRDL, F-56100, Lorient, France
[2]CEMMPRE, Department of Mechanical Engineering, University of Coimbra, Polo II, Rua Luís Reis Santos, Pinhal de Marrocos, 3030-788 Coimbra, Portugal

[*]E-mail: adrien.boyer@univ-ubs.fr

Abstract. The equibiaxial expansion test allows the evaluation of the mechanical behaviour of materials on a large strain range. In this context, a bulge test device was developed which enables a fast heating stage, a uniform heating of the specimen, and the control of the temperature during the expansion phase. Although during the test, the temperature is uniform at the pole of the cap, the contact with the tools imposes a gradient along its radius. Therefore, a thermo-mechanical model of the bulge test was built in order to improve knowledge about the influence of the temperature gradient in the evaluation of the hardening behaviour at the pole of the cap. Numerical simulations of the bulge test were performed considering both isothermal and anisothermal conditions. The anisothermal conditions considered reproduce the temperature gradient observed experimentally. This enables the analysis of the impact of the thermal gradient in the stress *versus* strain evolution at the pole of the cap and the comparison with experimental results.

1. Introduction

Nowadays, the quest for lightweight vehicles is fundamental to guarantee environmental sustainability. The norms imposed from environmental and safety agencies are particularly strong for the automotive industry, which has led to the development of materials with an improved ratio between strength and weight, or new-forming processes. In this context, aluminium alloys are increasingly used in the automotive industry. However, they are known for being more prone to springback phenomenon than conventional steels and to present lower formability than these steels, at room temperature. Such problems can be overcome using warm forming processes, *i.e.* by performing the deep drawing operation at an intermediate temperature, below the recrystallization temperature. These new forming conditions require either new material characterization methods or the current methods need to be adapted to high temperature conditions.

This study focus on the possibility of performing the characterization of the hardening behaviour of the materials using the equibiaxial expansion test in temperature. The material under analysis is the EN AW 6061-T6 alloy (initial thickness of 0.98 mm), for which experimental uniaxial tensile tests were previously performed on a Gleeble machine [1].

2. Experimental procedure

The setup used to perform the bulge test is presented in figure 1. A circular blank with a diameter of 240 mm is clamped into a blank holder and die, both electrically isolated and with a ceramic drawbead. The specimen is heated using the Joule's effect. Three pairs of electrodes are used with an electrical current intensity that can go up to 6000 A. Each pair is activated in a rotary manner as described in [2]. This device allows a fast heating stage, a uniform heating of the specimen, and the control of the temperature during the expansion phase. The heating is conducted in three phases, where the first one is a fast heating to the testing temperature, followed by a homogenization phase. Then, the temperature of the specimen is maintained during the expansion phase of the experiment, while an argon inert gas is used to deform the specimen. A type K thermocouple, welded on the blank centre by capacitive discharge, is used to control and monitor the temperature of the blank.

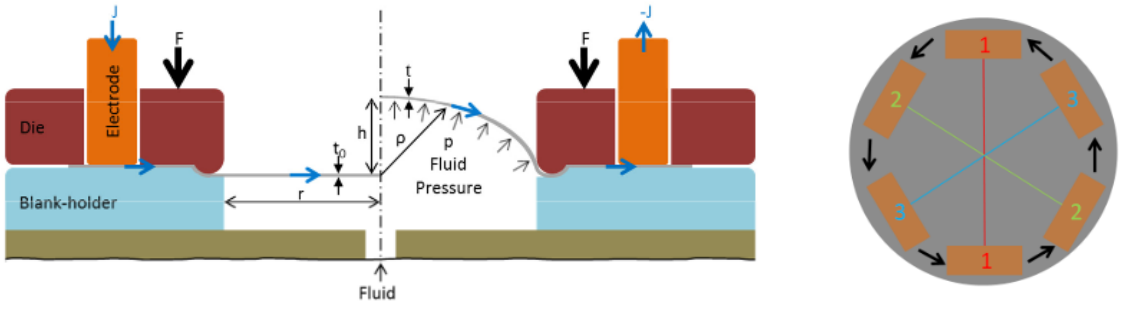

a) b)

Figure 1. The bulge expansion device used, a) Principle of the expansion device using Joule's effect to heat the blank, b) Rotary activation of the three pairs of electrodes.

The bulge tools are mounted in an Instron 8803 tensile test machine equipped with a 500 kN load cell. The die diameter is 120 mm and its fillet radius is 5 mm, following the recommendations of the standard ISO 16808:2014 [3]. Thus, the device can be used for sheets with an initial thickness up to 1.4 mm. The strain field at the pole is monitored with the Aramis-4M DIC system. A TESCOM ER5000 pressure controller is used as well as a 0-70 bars pressure sensor located inside the cavity to monitor the pressure. Figure 2 presents a scheme of the bulge test highlighting the definition of the bulge pole's height, h; the die cavity radius, a; the die fillet radius, df; the blank initial thickness, t_0; the pole thickness, t; and the bulge pole radius of curvature, ρ.

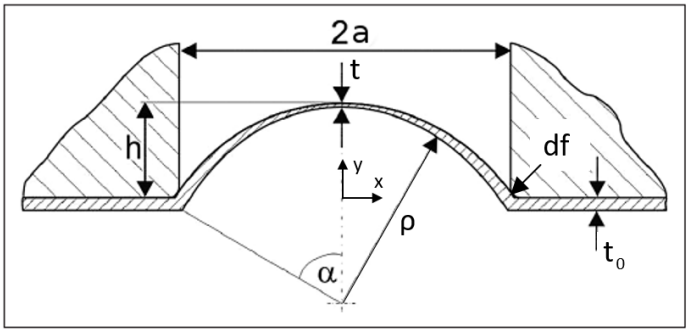

Figure 2. Bulge test scheme highlighting the relevant parameters.

The evaluation of the stress evolution during the test is based on the classical membrane theory, which relates the stress to the thickness (t) and radius of curvature of the blank's apex (ρ) as follows:

$$\sigma_{membrane} = \frac{P\rho}{2t} \quad (1)$$

where P is the pressure applied. When using a DIC system, the thickness strain at every instant can be evaluated using the acquired principal strains at the pole, by applying the volume conservation. The evolution of the radius of curvature is computed by fitting a sphere to the surfaces points using a least square method, which assumes equal radii of curvature along the rolling and the transverse directions. Although some authors report differences in these radii [4], for the EN AW 6061-T6 alloy under analysis

the planar anisotropy coefficient is close to zero [1], leading to a negligible difference in the radii of curvature for these directions.

The bulge tests were performed for the EN AW 6061-T6 alloy at 200°C considering five thermocouples, welded at initial positions from the centre of 5, 15, 30, 40 and 50 mm, enabling the acquisition of the temperature evolution during the test as well as the spatial gradient.

3. Finite element model for the bulge test

All numerical simulations were performed with the in-house solver DD3IMP, originally developed to simulate isothermal sheet metal forming processes [5] and that has been continuously updated to enable an improved description of the contact conditions [6][7] and the simulation of warm-forming processes. The thermomechanical problem is solved using the staggered coupled strategy proposed by Martins *et al.* [8]. The experimental setup heats the specimen using the joule's effect. However, in this study, the numerical modelling of the heat generated by electrical current was carried out through an energy rate generation in the volume of the specimen, which was evaluated in each increment to assure the user-prescribed constant heating rate. In the following sections, the details about the modelling of the mechanical behaviour of the EN AW 6061-T6 alloy and the tests conditions considered are given.

3.1. Material Behaviour

In order to describe the work hardening of aluminium alloys, it is normally recommended to use a phenomenological Hockett–Sherby type law, to enable the description of the saturation behaviour. The strain rate dependency is commonly introduced using a power law, as initially proposed by Wagoner *et al*. [9] and used in [10][11]. Under these assumptions, the yield stress, σ_y, evolves with temperature T and strain rate $\dot{\varepsilon}$ as follows:

$$\sigma_y(T,\dot{\varepsilon}) = [\sigma_0 + Q(1-\exp(-b(\bar{\varepsilon}^p)^n))]\left[\frac{\dot{\varepsilon}}{\dot{\varepsilon}_0}\right]^m \tag{2}$$

where $\bar{\varepsilon}^p$ is the equivalent plastic strain, σ_0 is the initial yield stress, Q is the maximum change in size of the yield surface, b denotes the growth rate of the yield surface (or the hardening), n is strain hardening coefficient, $\dot{\varepsilon}_0$ is a constant strain rate normalization factor and m is the strain rate sensitivity coefficient.

The temperature dependence was modelled by taking Q, b, n and m to be functions of the temperature. The strain rate sensitivity index m evolves exponentially with the temperature as follows:

$$m(T) = m_0 \exp\left(m_1 \frac{T}{T_m}\right) \tag{3}$$

where m_0 and m_1 are material parameters and T_m is the material melting temperature, which can be assumed to be equal to 600ºC for aluminium alloys. The strain-hardening index n was assumed to evolve linearly with temperature:

$$n(T) = n_0 - n_1\left(\frac{T}{T_m}\right) \tag{4}$$

where n_0 and n_1 are material parameters. The evolution of the size of the yield surface with the temperature is given by the following equation:

$$Q(T) = Q_0 + a_1\left[1-\exp\left(a_2\frac{T}{T_m}\right)\right] \tag{5}$$

where Q_0, a_1 and a_2 are material parameters. In the original formulation of the hardening law, it is assumed that, σ_0 is constant (see equation (1)). However, as shown in figure 3, this assumption is not valid for the EN AW 6061-T6 alloy. Therefore, a quadratic evolution was considered:

$$\sigma_0(T) = \sigma_0 - s_1\left(\frac{T}{T_m}\right) - s_2\left(\frac{T}{T_m}\right)^2 \tag{6}$$

where σ_0, s_1 and s_2 are material parameters. Thus, the identification procedure took into account a total of 12 parameters: $\dot{\varepsilon}_0$, b, m_0, m_1, n_0, n_1, Q_0, a_1, a_2, σ_0, s_1 and s_2. The parameters were identified by minimizing the difference between the experimental [1] and the numerical stress-strain curves, using a Generalized Reduced Gradient (GRG) algorithm and a two-step procedure described in [11]. The

parameters identified are presented in table 1. Figure 3 shows the comparison between the experimental and numerical results, highlighting that the modified Hockett-Sherby law enables an accurate description of the material behaviour.

Table 1. Modified Hockett-Sherby hardening law parameters.

Parameter	Value	Parameter	value
$\dot{\varepsilon}_0$	$1.0\times10^{-4}s^{-1}$	n_1	0.63
σ_0	272.1 MPa	Q_0	230.3 MPa
b	3.2	a_1	116.4 MPa
m_0	4.3×10^{-6}	a_2	2.7
m_1	26.1	s_1	0.0 MPa
n_0	0.80	s_2	795.3 MPa

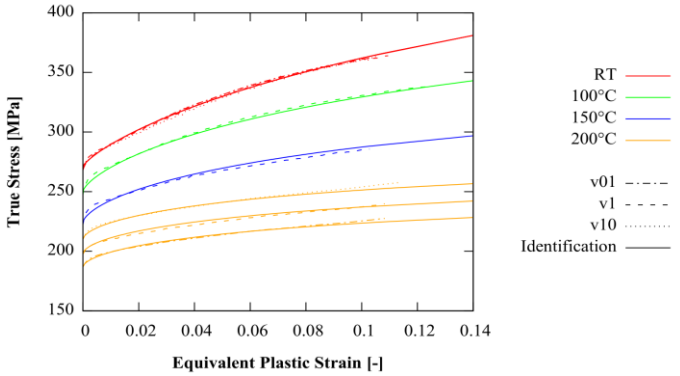

Figure 3. Comparison between experimental [1] and analytical stress-strain curves.

The elastic behaviour was assumed isotropic, described by the Generalized Hooke law. Although previous results show that the Young modulus of aluminium alloys decreases with the temperature increase, this effect was neglected in the numerical model. The other mechanical and thermal properties were also assumed as constant, as shown in table 2. The plastic behaviour was also assumed isotropic, described by the von Mises yield criterion.

Table 2. Mechanical and thermal properties of the EN AW 6061-T6 aluminium alloy.

Parameter	Value
Young Modulus	68900 MPa
Poisson's ratio	0.33
Density	2700 kg/m^3
Specific Heat Capacity	900 J/kg/K
Thermal Conductivity	3 W/m/K

3.2. Numerical procedure

Due to geometrical and material symmetry conditions, it was decided to consider only a quarter of the model as shown in figure 4. The tools are assumed as rigid and, consequently, only the surfaces in contact with the blank are described. Figure 4 shows the coarse discretization adopted for the tools, since Nagata patches are used to assure a smooth interpolation [12]. The blank is discretized with a total of 11523 nodes and 7440 hexahedral linear finite elements. Two layers are considered through the thickness and the central zone is discretized with a relative fine structured mesh, since it corresponds to the zone of interest. The same mesh is used for the mechanical and the thermal problems. However, full integration is adopted in the thermal problem, while the mechanical resorts to the selective reduced integration technique.

The model shown in figure 4 is used for both isothermal and anisothermal conditions. The pressure is applied to the bottom of the blank, considering a linear increase over time. However, for anisothermal conditions, it is also necessary to model the heat losses. The thermal conductance between the sheet and

the tools will promote heat losses, as long as the tools present a different temperature than the blank. Based on previous numerical results, regarding the analysis of the heating stage for a boron steel [13], it was decided to keep the tools at room temperature. Note that it is very difficult to evaluate the coefficients that characterize the thermal conductance. From the numerical point of view, this heat loss is usually modelled as convection taking place on the contact interface, where the interfacial heat transfer coefficient (h_c) is the main parameter. In this work it was decided to adopt the same function presented in [14], which states that the heat flux due to thermal conductance is given by:

$$\dot{q}_c = h_c(T_{\text{blank}} - T_{\text{tool}}) = \left[h_{\text{sup}}\exp(-m_c g_n)\right](T_{\text{blank}} - T_{\text{tool}}), \quad (7)$$

where T_{blank} and T_{tool} correspond to the blank and the tool temperature, respectively. Moreover, h_c depends on the distance (g_n) between the blank and the tools, such that when contact occurs it attains an upper threshold value (h_{sup}) that decreases exponentially with the increase of the gap distance. m_c is the parameter used to control the rate of decrease with g_n. This allows obtaining a smooth variation of the heat transfer coefficient between contact and non-contact (free convection) areas. In this study the values used for these parameters were: h_{sup}=1 W/m^2.K and m = 8.59. Moreover, convection heat losses were also considered between the blank top surface and the surrounding air (h_{air}) and the blank bottom surface and the argon inert gas (h_{gas}). These convection coefficients were determined based on a trial and error approach, until obtaining a proper adjustment between the experimental and numerical temperature evolution during the test, for the five locations of thermocouples previously mentioned. In this study the value used were: h_{air}=0.0195 W/m^2.K and h_{gas}=0.03 W/m^2.K.

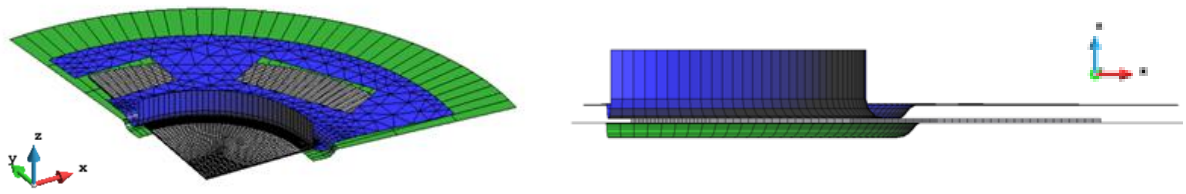

Figure 4. Schematic representation of one quarter of the model: blank (grey) and initial position of the blank holder (green) and die (blue).

The anisothermal test conditions try to replicate the experimental test. Therefore, in the first phase the blank holder is moved against the die until attaining a maximum force of 75kN (one quarter of the total force, due to symmetry conditions). The second phase corresponds to the heating of the blank until the value of 200 ºC is attained at the centre of the blank. Then, the third phase corresponds to the temperature homogenization. Finally, the fourth phase corresponds to the forming one, with a linear increase of pressure, until a maximum value of 5 MPa is attained. Nevertheless, it should be pointed out that the cooling and springback phases were not considered in this work. The isothermal test conditions impose that the initial temperature of the blank and the tools is already 200ºC. Thus, the test involves only the blank holder clamping phase and the forming one, considering the same maximum blank holder force and pressure values as for the anisothermal test.

3.3. Temperature distribution

Figure 5a) shows the temperature distribution in the blank at the end of the heating phase for the anisothermal test. It is possible to observe that in the centre region the temperature is quite uniform. However, since the tools are electrically isolated, they remain at the room temperature, which generates a temperature gradient mostly due to the heat losses by thermal conductance.

The comparison between the experimental and the numerical temperature evolution during the test is presented in figure 5b). As previously mentioned, the convection coefficients were determined trying to minimize the difference between those results. Therefore, as expected, there is a good correlation between them. However, it should be mentioned that the points located at a distance higher than 15 mm

show a decreasing trend at the end of the bulging phase that is not observed in the experimental data. This suggests that the interfacial heat transfer coefficient can be overestimated.

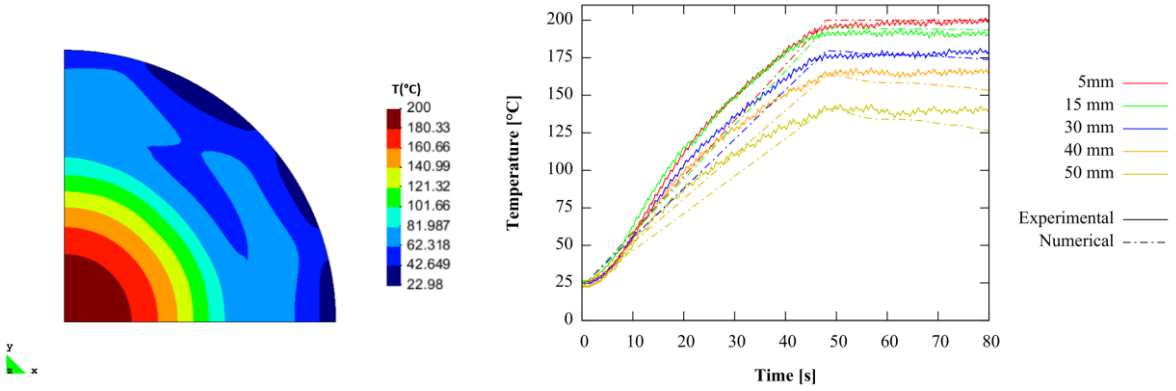

a) b)

Figure 5. Anisothermal test conditions: a) Temperature distribution at the end of the heating phase; b) Comparison between the experimental and the numerical temperature evolution during the test, for nodes located at the same initial positions of the thermocouples used in the experimental test.

4. Results analysis and discussion

Figure 6a) presents the evolution of the pressure in function of the pole's vertical displacement for isothermal, anisothermal and experimental conditions. The pressure value required to attain the same vertical displacement is higher for the anisothermal conditions. This is connected with the fact that the isothermal conditions promote a more homogenous strain field, as the whole blank surface is heated to 200°C. On the other hand, for anisothermal conditions the temperature gradient (see figure 5) induces a higher strain localization at the blank's apex, due to the gradient of material properties (see figure 3). Globally, the anisothermal case reproduces well the experimental pressure evolution, indicating a good description of the material behaviour. Figure 6b) presents the evolution of the thickness at the blank's apex, as predicted by the isothermal and the anisothermal models and the experimental result. Globally, both numerical tests underestimate the thickness reduction when compared to the experimental. This may be connected with the adoption of the von Mises yield criterion, since it was observed that the alloy presents a normal anisotropy coefficient lower than 1 [15]. Nevertheless, the anisothermal conditions predict a trend closer to the experimental one, which may be related with the higher localization of the deformation at the blank's apex.

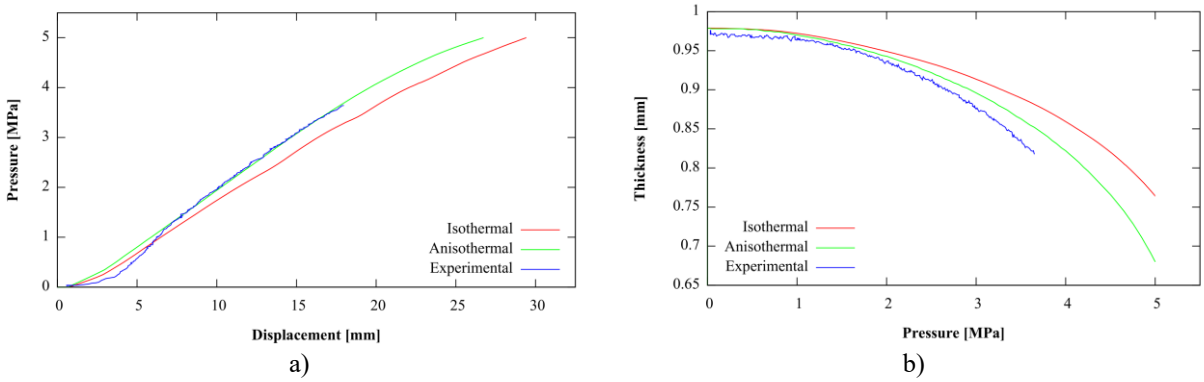

a) b)

Figure 6. Comparison between isothermal, anisothermal and experimental conditions: a) Evolution of the pressure in function of the pole's vertical displacement; b) Evolution of the thickness in the centre of the blank in function of the pressure.

Figure 7a) shows the evolution of the stress in function of the equivalent plastic strain, as predicted for the integration point (Gauss point) located closer to the mentioned distance to the centre. The stress-strain evolution is mainly dictated by the blank's temperature. Therefore, all points of the isothermal

test follow a similar curve, while for anisothermal conditions the points located further away from the centre present higher yield stress values (see also figure 3). The vertical lines mark the maximum values attained for the strain, highlighting that, for each distance, the anisothermal condition leads to higher equivalent plastic strain values. This is connected with the different geometry of the blank surface, since a larger height at the apex is attained (see figure 6), which means that there is an increase of surface area along the blank radius to accommodate the strain localization at the pole.

The evolution of the strain-rate in function of the equivalent plastic strain is presented in figure 7b), for the same points. It is observed that the influence of the temperature gradient is marginal, with the strain rate showing a linear increase with equivalent plastic strain in logarithmic scale. The range for the strain-rate is approximately from $1x10^{-4}$ to $1x10^{-1}s^{-1}$, with a monotonous increase resulting in a smooth evolution of the stress curve, as shown in figure 7a) for both conditions.

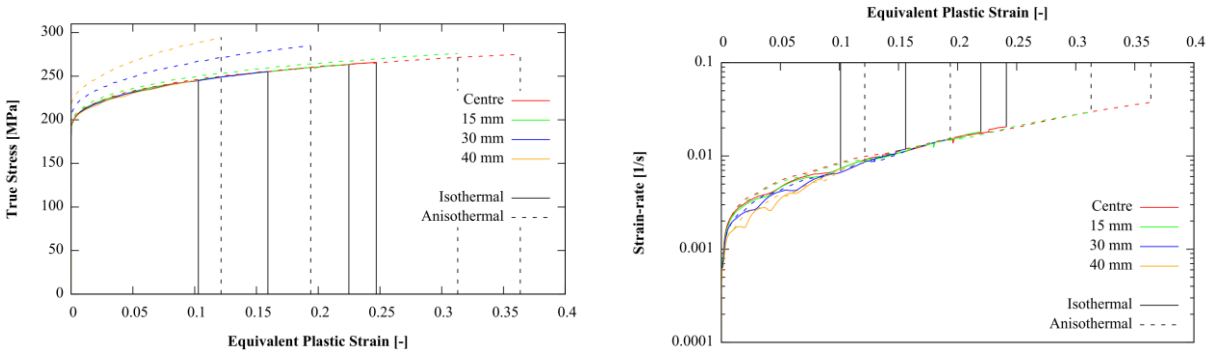

a) b)

Figure 7. Comparison between isothermal and anisothermal conditions: a) Evolution of the stress with the equivalent plastic strain; b) Evolution of the strain-rate with the equivalent plastic strain.

The evolution of the true stress in function of the equivalent plastic strain for the integration point located closer to the specimen apex is presented in figure 8. This figure also shows the yield stress evolution (see equation (2)) for 200°C and the two extreme values of strain rate observed in figure 7b), to highlight the influence of the evolution of the strain rate on the hardening behaviour. Moreover, the experimental results are also presented. The comparison between the experimental and the numerical results indicates that the strain rate increase is higher in the experimental results, which is consistent with the thickness evolution presented in figure 6.

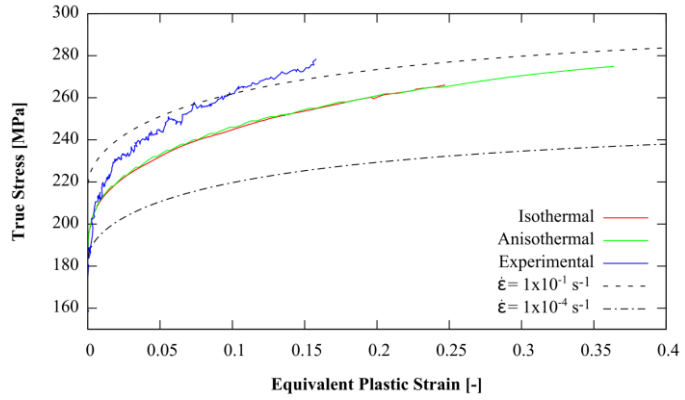

Figure 8. Comparison between numerical, analytical (for 200°C and constant strain rate values of $1x10^{-4}s^{-1}$ and $1x10^{-1}$), and experimental results for the evolution of the true stress in function of the equivalent plastic strain.

5. Conclusion

The thermomechanical behaviour of the EN AW 6061-T6 alloy was described using a modified Hockett-Sherby hardening law, based on experimental results extracted from uniaxial tensile tests, performed in a Gleeble device. The temperature gradient observed in the blank during the experimental bulge test at 200°C was analysed and an anisothermal model was built using the in-house finite-element solver DD3IMP. The same code was used to perform an isothermal numerical analysis of the process.

Globally, the identified hardening law enabled an accurate prediction of the evolution of the specimen geometry during the bulge test, particularly for anisothermal conditions. Both numerical models predict a similar exponential increase of the strain-rate during the bulge test. This evolution of the strain-rate influences the hardening observed for the stress-strain curves, due to the positive strain-rate sensitivity of the material. The knowledge acquired will contribute to improve the analysis of the bulge test at warm temperature for the EN AW 6061-T6 and potentially other materials.

Acknowledgements

The authors would like to acknowledge the funding that sponsored this research work: the national funds from the French Ministry of Higher Education and the Portuguese Foundation for Science and Technology (FCT) via the projects Materiais e Tecnologias Industriais Sustentaveis (MATIS) CENTRO-01-0145-FEDER-000014 and UIDB/00285/2020.

References

[1] V. M. Simões, M. C. Oliveira, H. Laurent, and L. F. Menezes, "The punch speed influence on warm forming and springback of two Al-Mg-Si alloys," *J. Manuf. Process.*, vol. 38, pp. 266–278, Feb. 2019, doi: 10.1016/j.jmapro.2019.01.020.

[2] N. Demazel *et al.*, "Simulations of joule effect heating in a bulge test," in *AIP Conference Proceedings*, 2016, vol. 1769.

[3] "ISO16808:2014 : Metallic materials -- Sheet and strip -- Determination of biaxial stress-strain curve by means of bulge test with optical measuring systems." International Organization for Standardization, Aug. 2014, [Online]. Available: https://www.iso.org/standard/57777.html.

[4] J. Min, T. B. Stoughton, J. Carsley, B. E. Carson, J. Lin, and X. Gao, "Accurate characterization of biaxial stress-strain response of steel metal from bulge testing," *Int J Plast Artic.*, no. 94, pp. 1–22, 2016, doi: https://doi.org/10.1016/j.ijplas.2016.02.005.

[5] L. F. Menezes and C. Teodosiu, "Three-dimensional numerical simulation of the deep-drawing process using solid finite elements," *J. Mater. Process. Technol.*, vol. 97, no. 1–3, pp. 100–106, 2000, doi: 10.1016/s0924-0136(99)00345-3.

[6] M. C. Oliveira, J. L. Alves, and L. F. Menezes, "Algorithms and Strategies for Treatment of Large Deformation Frictional Contact in the Numerical Simulation of Deep Drawing Process," *Arch. Comput. Methods Eng.*, vol. 15, no. 2, pp. 113–162, Jun. 2008, doi: 10.1007/s11831-008-9018-x.

[7] D. M. Neto, M. C. Oliveira, and L. F. Menezes, "Surface smoothing procedures in computational contact mechanics," *Arch. Comput. Methods Eng.*, vol. 24, no. 1, pp. 37–87, 2017, doi: 10.1007/s11831-015-9159-7.

[8] J. M. P. Martins *et al.*, "A new staggered algorithm for thermomechanical coupled problems," *Int. J. Solids Struct.*, vol. 122, pp. 42–58, 2017.

[9] R. H. Wagoner, E. Nakamachi, and Y. Germain, "Analysis of sheet forming operations using the finite element method," Toronto, 1988.

[10] H. Laurent, J. Coër, P.-Y. Manach, M. C. Oliveira, and L. F. Menezes, "Experimental and numerical studies on the warm deep drawing of an Al–Mg alloy," *Int. J. Mech. Sci.*, 2015.

[11] M. C. Oliveira, L. Germain, H. Laurent, D. M. Neto, J. L. Alves, and L. F. Menezes, "A modified Hockett-Sherby law enabling the description of the thermomechanical behaviour of the AA6061-T6," 2020, vol. 47, pp. 896–903, doi: 10.1016/j.promfg.2020.04.277.

[12] D. M. Neto, M. C. Oliveira, L. F. Menezes, and J. L. Alves, "Applying Nagata patches to smooth discretized surfaces used in 3D frictional contact problems," *Comput. Methods Appl. Mech. Eng.*, vol. 271, pp. 296–320, doi: 10.1016/j.cma.2013.12.008.

[13] A. Boyer, "Essais d'expansion à haute température sur un acier trempant," Master's thesis, Université Bretagne Sud, Lorient, France, 2017.

[14] D. M. Neto, M. Pais, M. C. Oliveira, J. L. Alves, and L. F. Menezes, "Thermomechanical analysis of the draw bead test," *Adv. Mater. Process. Technol.*, vol. 5, no. 3, pp. 401–417, 2019.

[15] V. M. Simões, H. Laurent, M. Oliveira, and L. Menezes, "The influence of warm forming in natural aging and springback of Al-Mg-Si alloys," *Int. J. Mater. Form.*, vol. 12, no. 1, pp. 57–68, Jan. 2019, doi: 10.1007/s12289-018-1406-7.